



## Dark path holonomic qudit computation

Tomas André  and Erik Sjöqvist <sup>\*</sup>

*Department of Physics and Astronomy, Uppsala University, Box 516, Se-751 20 Uppsala, Sweden*



(Received 5 August 2022; accepted 18 November 2022; published 2 December 2022)

Nonadiabatic holonomic quantum computation is a method used to implement high-speed quantum gates with non-Abelian geometric phases associated with paths in state space. Due to their noise tolerance, these phases can be used to construct error resilient quantum gates. We extend the holonomic dark path qubit scheme in [M.-Z. Ai *et al.*, *Fundam. Res.* **2**, 661 (2022)] to qudits. Specifically, we demonstrate one- and two-qudit universality by using the dark path technique. Explicit qutrit ( $d = 3$ ) gates are demonstrated and the scaling of the number of loops with the dimension  $d$  is addressed. This scaling is linear and we show how any diagonal qudit gate can be implemented efficiently in any dimension.

DOI: [10.1103/PhysRevA.106.062402](https://doi.org/10.1103/PhysRevA.106.062402)

### I. INTRODUCTION

The most common form of quantum computation is the circuit model, which is analogous to the circuits used for classical computers. Gates are replaced by unitary transformations (quantum gates) and bits by qubits. To achieve the computational advantage it is important to construct robust, noise-resilient quantum gates. A candidate for this is holonomic quantum computation [1,2], which is based on non-Abelian (matrix-valued) geometric phases in adiabatic [3] or nonadiabatic [4] evolution. Such holonomic gates are only dependent on the geometry of the system's state space and thus are resilient to local errors in the quantum evolution. Recent theoretical and experimental advances in holonomic quantum computation can be found in Refs. [5–13] and [14–21], respectively.

The idea that elements of computation should be limited to qubits is sort of an arbitrary choice that most likely rose out of convenience due to binary logic. So why binary logic? It is simply the easiest nontrivial example: in binary logic, things can be either 0 or 1, True or False, **on** or **off**, etc. Due to its simplicity, it is no wonder that this is how the first computer was designed. But are we limited to bits? As early as 1840, a mechanical trinary (three-valued logic) calculation device was built by Fowler [22], and in 1958 the first electronic trinary computer was developed by the Soviet Union [23]. Although the trinary computer had many advantages over the binary one, it never saw the same widespread success. However, there is nothing in theory that forbids a higher-dimensional computational basis, even more so when it comes to quantum

computers, where the implementation of the elements of computation already surpasses the simplicity of **on** and **off**. Indeed, qudits have been implemented experimentally and shown definite advantages [24,25] as well as paving the way for achieving large-scale quantum computation [26]. Thus, one may consider  $d$  dimensional qudits as primitive units of quantum information, with promising results that show potential, some of them reviewed in Ref. [27].

Here, we develop a qudit generalization of the idea of dark paths proposed in Ref. [21] for implementing nonadiabatic holonomic qubit gates. By this, we combine the advantages of improved robustness associated with the dark path approach with the enlarged encoding space and improved gate efficiency of higher-dimensional quantum information units [27]. In the next two sections, we extend the dark path idea to the qutrit ( $d = 3$ ). We examine the robustness of the  $d = 3$  gates to systematic errors in the Rabi frequencies of the laser induced transitions. The case of general  $d$  is examined in Secs. IV and V. The paper ends with the conclusions.

### II. DARK PATH SETTING

The key point of the qutrit dark path setting is to look for a level structure with three ground states  $|k\rangle$ ,  $k = 1, 2, 3$ , encompassing a single fixed (time-independent) dark eigenstate, as well as an extra fourth auxiliary lower level  $|a\rangle$ . As the number of dark eigenstates in the computational qutrit subspace  $\text{Span}\{|1\rangle, |2\rangle, |3\rangle\}$  equals the difference between the number of excited states and the number of ground states [28], this amounts to coupling the ground state levels to two excited states  $|e_1\rangle, |e_2\rangle$ . The desired coupling structure is described by the Hamiltonian (see left panel of Fig. 1)

$$H^{(3)} = \sum_{k=1}^3 \sum_{l=1}^2 \omega_{k,l} |k\rangle \langle e_l| + \frac{\Omega_a(t)}{2} |a\rangle \langle e_2| + \text{H.c.}, \quad (1)$$

with  $\omega_{3,1} = 0$ . Laser-induced dipole transitions between hyperfine levels of trapped ions provide an ideal platform for realizing such coupling structures [29]. The specific

<sup>\*</sup>erik.sjoqvist@physics.uu.se

*Published by the American Physical Society under the terms of the Creative Commons Attribution 4.0 International license. Further distribution of this work must maintain attribution to the author(s) and the published article's title, journal citation, and DOI. Funded by Bibsam.*

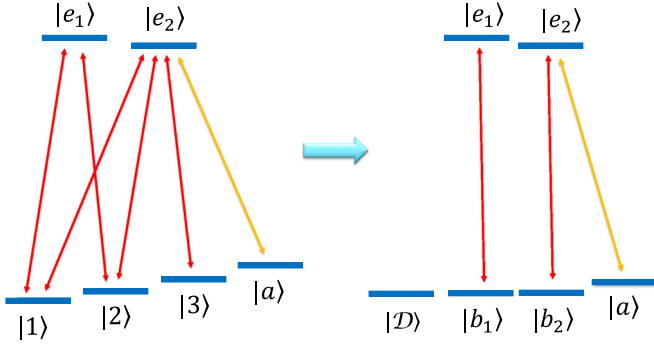


FIG. 1. Level setting for realizing a dark path holonomic qutrit gate (left panel). The specific coupling structure may be realized by inducing transitions between hyperfine levels in trapped ions. It allows for a Morris-Shore transformation [30] applied to the qutrit levels  $|1\rangle$ ,  $|2\rangle$ ,  $|3\rangle$ , resulting in a single dark energy eigenstate  $|\mathcal{D}\rangle$  and two bright states  $|b_1\rangle$ ,  $|b_2\rangle$ , while leaving the auxiliary state  $|a\rangle$  untouched (right panel).

Hamiltonian  $H^{(3)}$  allows for a Morris-Shore transformation [30] applied to the qutrit levels  $|1\rangle$ ,  $|2\rangle$ ,  $|3\rangle$  only, yielding (see right panel of Fig. 1)

$$H^{(3)} = \sum_{k=1}^2 \frac{\Omega_k(t)}{2} e^{-i\phi_k} |b_k\rangle \langle e_k| + \frac{\Omega_a(t)}{2} |a\rangle \langle e_2| + \text{H.c.}, \quad (2)$$

with  $\Omega_k$  being real-valued time-dependent Rabi frequencies and  $\phi_k$  time-independent phases, by employing the dark-bright basis

$$\begin{aligned} |\mathcal{D}\rangle &= \cos\theta |1\rangle + e^{i\chi} \sin\theta \cos\varphi |2\rangle + e^{i\xi} \sin\theta \sin\varphi |3\rangle, \\ |b_1\rangle &= \frac{1}{\sqrt{1 - \sin^2\theta \sin^2\varphi}} (-e^{-i\chi} \sin\theta \cos\varphi |1\rangle + \cos\theta |2\rangle), \\ |b_2\rangle &= \frac{1}{\sqrt{1 - \sin^2\theta \sin^2\varphi}} [\sin\theta \cos\theta \sin\varphi |1\rangle \\ &\quad + e^{i\chi} \sin^2\theta \sin\varphi \cos\varphi |2\rangle + e^{i\xi} (\sin^2\theta \sin^2\varphi - 1) |3\rangle], \end{aligned} \quad (3)$$

where  $|\mathcal{D}\rangle$  is a dark energy eigenstate satisfying  $H^{(3)}|\mathcal{D}\rangle = 0$ . Note that  $|\mathcal{D}\rangle$ ,  $|b_1\rangle$ ,  $|b_2\rangle$  span the computational subspace, i.e.,  $\text{Span}\{|\mathcal{D}\rangle, |b_1\rangle, |b_2\rangle\} = \text{Span}\{|1\rangle, |2\rangle, |3\rangle\}$ . The original  $\omega_{k,l}$  can be expressed in the parameters  $\theta$ ,  $\varphi$ ,  $\chi$ ,  $\xi$  by expanding the bright states on the right-hand side of Eq. (2) in terms of the original qutrit levels  $|k\rangle$  and by comparing with Eq. (1).

A pair of dark path states  $|D_1(t)\rangle$ ,  $|D_2(t)\rangle$  can now be defined. These states should satisfy two conditions: (i) they should be orthogonal to  $|\mathcal{D}\rangle$ , and (ii) their average energy  $\langle D_k(t)|H_d|D_k(t)\rangle$ ,  $k = 1, 2$ , should vanish along their evolution paths. Explicitly, one may check that

$$\begin{aligned} |D_1(t)\rangle &= \cos u(t) e^{-i\phi_1} |b_1\rangle + i \sin u(t) |e_1\rangle, \\ |D_2(t)\rangle &= \cos u(t) \cos v(t) e^{-i\phi_2} |b_2\rangle - i \sin u(t) |e_2\rangle \\ &\quad - \cos u(t) \sin v(t) |a\rangle \end{aligned} \quad (4)$$

satisfy the dark path conditions. In fact, these states even satisfy the stronger condition [2]  $\langle D_1(t)|H_d|D_2(t)\rangle = 0$ , which opens up for holonomic gates provided the

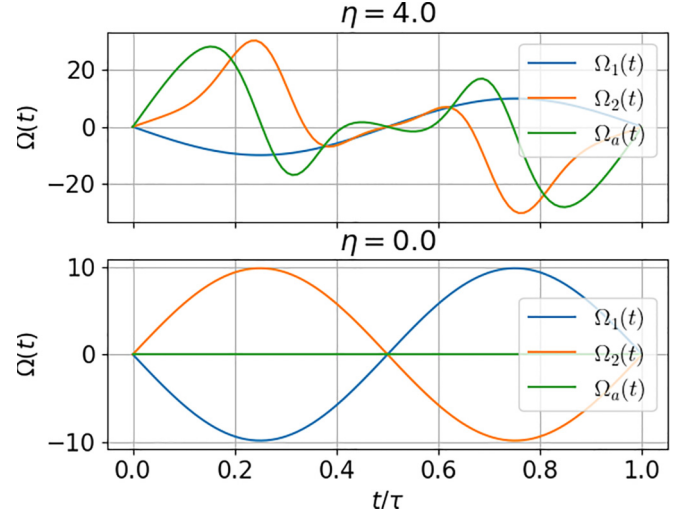


FIG. 2. Rabi frequencies in the qutrit scheme for zero and nonzero value of  $\eta$ . Note that only  $\Omega_2(t)$  and  $\Omega_a(t)$  change shape with  $\eta$ . This extends to the higher-dimensional case in that only the pulse with the largest index and  $\Omega_a(t)$  depend on  $\eta$  for arbitrary  $d$  [see Eq. (20) below].

parameters  $u(t)$ ,  $v(t)$  are chosen such that the qutrit subspace  $\text{Span}\{|\mathcal{D}\rangle, |D_1(t)\rangle, |D_2(t)\rangle\}$  evolves in a cyclic manner, i.e., that  $\text{Span}\{|\mathcal{D}\rangle, |D_1(\tau)\rangle, |D_2(\tau)\rangle\} = \text{Span}\{|1\rangle, |2\rangle, |3\rangle\}$  for some run time  $\tau$ . This is achieved provided  $u(\tau) = u(0) = v(\tau) = v(0) = 0$  so that each dark path starts in the respective bright state and travels along a curve and returns to the same bright state at  $t = \tau$ .

One may now use the Schrödinger equation to reverse engineer the time-dependent parameters  $\Omega_l(t)$ . A calculation yields

$$\begin{aligned} \Omega_1(t) &= -2\dot{u}(t), \\ \Omega_2(t) &= 2[\dot{v}(t) \cot u(t) \sin v(t) + \dot{u}(t) \cos v(t)], \\ \Omega_a(t) &= 2[\dot{v}(t) \cot u(t) \cos v(t) - \dot{u}(t) \sin v(t)]. \end{aligned} \quad (5)$$

We follow Ref. [21] and choose

$$u(t) = \frac{\pi}{2} \sin^2 \frac{\pi t}{\tau}, \quad v(t) = \eta[1 - \cos u(t)], \quad (6)$$

which ensures cyclic evolution. The parameter  $\eta$  represents the coupling strength to the auxiliary state in the sense that  $|D_2(t)\rangle$  becomes independent of  $|a\rangle$  when  $\eta = 0$ . The shape of the Rabi frequencies with this choice of  $u$  and  $v$  are displayed in Fig. 2. This completes the dark path construction in the qutrit case.

### III. HOLONOMIC DARK PATH ONE-QUTRIT GATES

#### A. Gate construction

The multipulse single-loop setting [31] is used for dark path qutrit gates, thereby the loop is divided into two path segments by applying laser pulses. Explicitly, the pulses take the subspace  $\text{Span}\{|\mathcal{D}\rangle, |b_1\rangle, |b_2\rangle\}$  into  $\text{Span}\{|\mathcal{D}\rangle, |e_1\rangle, |e_2\rangle\}$  and back, by applying phase shifts  $\gamma_1$ ,  $\gamma_2$  to the second segment relative to the first one. Note that  $u(\frac{\tau}{2}) = \frac{\pi}{2}$ , which implies that the duration is  $\frac{\tau}{2}$  for both path segments. This results in

the unitaries

$$\begin{aligned}
 U\left(\frac{\tau}{2}, 0\right) &= |\mathcal{D}\rangle\langle\mathcal{D}| - i(|e_1\rangle\langle b_1| + |b_1\rangle\langle e_1|) \\
 &\quad - i(|e_2\rangle\langle b_2| + |b_2\rangle\langle e_2|), \\
 U\left(\tau, \frac{\tau}{2}\right) &= |\mathcal{D}\rangle\langle\mathcal{D}| + ie^{i\gamma_1}(|b_1\rangle\langle e_1| + |e_1\rangle\langle b_1|) \\
 &\quad + ie^{i\gamma_2}(|b_2\rangle\langle e_2| + |e_2\rangle\langle b_2|), \quad (7)
 \end{aligned}$$

restricted to the part with nontrivial action on the computational subspace. By combining these unitaries, we obtain the one-qutrit gate

$$\begin{aligned}
 U_3^{(1)} &= U\left(\tau, \frac{\tau}{2}\right)U\left(\frac{\tau}{2}, 0\right) \\
 &= |\mathcal{D}\rangle\langle\mathcal{D}| + e^{i\gamma_1}|b_1\rangle\langle b_1| + e^{i\gamma_2}|b_2\rangle\langle b_2|. \quad (8)
 \end{aligned}$$

The holonomy  $U_3^{(1)}$  can be parameterized by  $\chi, \xi, \theta, \varphi, \gamma_1, \gamma_2$ ; however, these parameters are not enough to construct all gates. For instance,  $X_3$  requires two loops. The full gate is given by repeating  $U_3^{(1)}$  with a different set of parameters,

$$U_3^{(1)} = U_3^{(1)}(\chi', \xi', \theta', \varphi', \gamma_1', \gamma_2')U_3^{(1)}(\chi, \xi, \theta, \varphi, \gamma_1, \gamma_2). \quad (9)$$

In this way, the following gates can be implemented:

$$\begin{aligned}
 X_3 &= U\left(0, 0, \frac{\pi}{4}, \frac{\pi}{2}, 0, \pi\right) \times U\left(0, 0, \frac{\pi}{2}, \frac{\pi}{4}, 0, \pi\right) \\
 &= \begin{pmatrix} 0 & 0 & 1 \\ 1 & 0 & 0 \\ 0 & 1 & 0 \end{pmatrix},
 \end{aligned}$$

$$Z_3 = U\left(0, 0, 0, 0, \frac{2\pi}{3}, \frac{4\pi}{3}\right) = \begin{pmatrix} 1 & 0 & 0 \\ 0 & e^{i\frac{2\pi}{3}} & 0 \\ 0 & 0 & e^{i\frac{4\pi}{3}} \end{pmatrix},$$

$$T_3 = U\left(0, 0, 0, 0, \frac{2\pi}{9}, \frac{-2\pi}{9}\right) = \begin{pmatrix} 1 & 0 & 0 \\ 0 & e^{i\frac{2\pi}{9}} & 0 \\ 0 & 0 & e^{-i\frac{2\pi}{9}} \end{pmatrix},$$

$$\begin{aligned}
 H_3 &= U(6.41 \times 10^{-4}, 6.56 \times 10^{-4}, 0.48, 0.79, 1.58, 1.56) \\
 &\quad \times U(9.81 \times 10^{-3}, 0.00, 1.187, 2.15, 0.00, 1.57) \\
 &\approx \frac{1}{\sqrt{3}} \begin{pmatrix} 1 & 1 & 1 \\ 1 & e^{i\frac{2\pi}{3}} & e^{i\frac{4\pi}{3}} \\ 1 & e^{i\frac{4\pi}{3}} & e^{i\frac{2\pi}{3}} \end{pmatrix}. \quad (10)
 \end{aligned}$$

The set includes qutrit equivalents of the Hadamard and  $T$  gate, which constitutes a universal set. Thus, no more than two loops for each gate are needed to achieve single-qutrit universality. Figures 3 and 4 show the population of the computational, excited, and auxiliary states during implementation of  $H_3$  and  $X_3$ , respectively, plotted against the dimensionless time  $t/\tau$ . To this end, a linear combination of  $|\mathcal{D}_1(t)\rangle$ ,  $|\mathcal{D}_2(t)\rangle$ , and  $|\mathcal{D}\rangle$  is matched at  $t = 0$  to a given initial state, and the populations are thereafter identified by monitoring the evolving state at  $t > 0$ . We have chosen  $\eta = 4.0$  in the simulations to allow for direct comparison with the qubit case analyzed in Ref. [21].

All diagonal gates can be parameterized by a single loop by fixing  $\theta = \varphi = \chi = \xi = 0$ . The dark-bright basis states

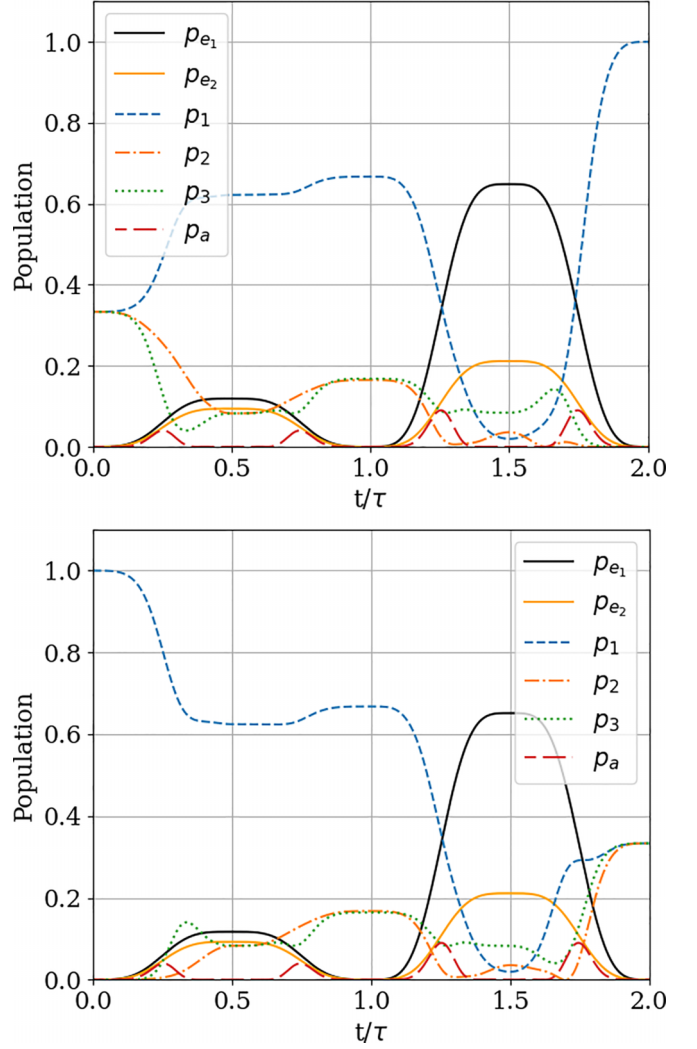


FIG. 3. The effect of the  $H_3$  gate on the initial states  $\frac{1}{\sqrt{3}}(|1\rangle + |2\rangle + |3\rangle)$  (upper panel) and  $|1\rangle$  (lower panel) plotted as a function of dimensionless time  $t/\tau$ . The coupling to the auxiliary state is  $\eta = 4.0$ . Note that since the plots show the populations of the computational, excited, and auxiliary states, phases cannot be seen.

reduce to  $|\mathcal{D}\rangle = |1\rangle$ ,  $|b_1\rangle = |2\rangle$ , and  $|b_2\rangle = -|3\rangle$ . By Eq. (8), one can thus see that all diagonal unitaries can be specified by  $\gamma_1$  and  $\gamma_2$ :

$$U_3^{(1)}(0, 0, 0, 0, \gamma_1, \gamma_2) = \begin{pmatrix} 1 & 0 & 0 \\ 0 & e^{i\gamma_1} & 0 \\ 0 & 0 & e^{i\gamma_2} \end{pmatrix}. \quad (11)$$

## B. Robustness test

We quantify gate robustness by means of fidelity

$$F(\psi, \tilde{\psi}) = |\langle\psi|\tilde{\psi}\rangle|, \quad (12)$$

with  $\psi$  and  $\tilde{\psi}$  the ideal and nonideal output states of the gate, given the same input. The fidelity is averaged by sampling initial states and letting them evolve with time by numerically solving the Schrödinger equation using the SciPy implementation of backwards differentiation [32].

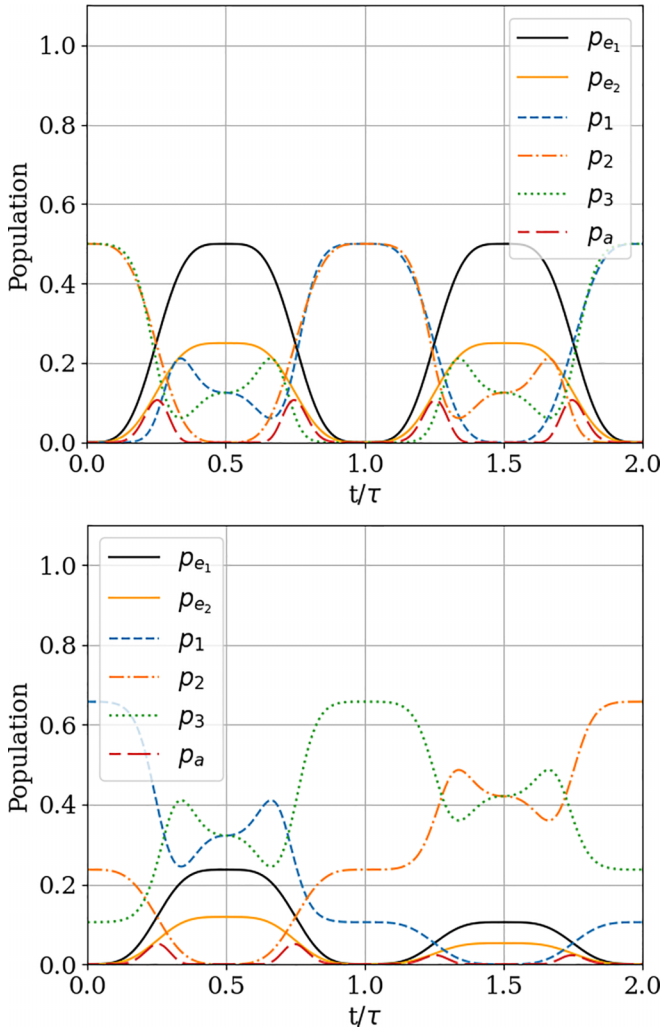


FIG. 4. The effect of the  $X_3$  gate on the initial states  $\frac{1}{\sqrt{2}}(|2\rangle + |3\rangle)$  (upper panel) and  $\frac{1}{\sqrt{38}}(5|1\rangle + 3|2\rangle + 2|3\rangle)$  (lower panel) plotted as a function of dimensionless time  $t/\tau$ . The coupling to the auxiliary state is  $\eta = 4.0$ . Note that since the plots show the populations of the computational, excited, and auxiliary states, phases cannot be seen.

We introduce systematic errors by shifting the Rabi frequencies  $\Omega_p \mapsto \Omega_p(1 + \delta)$  for  $p = 1, 2, a$  in Eq. (2) and compare to the exact solution obtained by applying the ideal gate to the initial state. The calculated fidelities are shown in Fig. 5. In the plots, it can be seen that coupling to the auxiliary state (again with  $\eta = 4.0$ ) improves the robustness to Rabi frequency errors compared to the standard nonadiabatic holonomic scheme ( $\eta = 0$ ). This result is similar to that found in Ref. [21] for the qubit case, and it is reasonable to expect that it applies for higher  $d$  as well. As qudits offer enlarged encoding space and improved gate efficiency [27], this result demonstrates potential for dark path holonomic qudit computation.

#### IV. QUDIT GENERALIZATION

To generalize the dark path scheme to arbitrary dimension  $d$ , we extend the above qutrit scheme by using  $d$  ground states  $|k\rangle$ ,  $d - 1$  excited states  $|e_l\rangle$ , and an auxiliary state  $|a\rangle$ . The

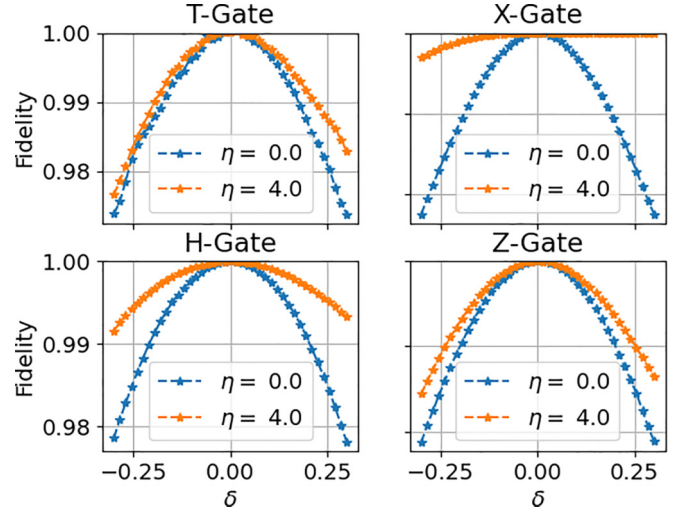


FIG. 5. Robustness test, average fidelity of the  $T_3$ ,  $X_3$ ,  $H_3$ , and  $Z_3$  gates. The averages are calculated by sampling over 500 randomized initial states with a perturbation  $\Omega \mapsto (1 + \delta)\Omega$  of the Rabi frequency.

dark path Hamiltonian

$$H^{(d)} = \sum_{k=1}^d \sum_{l=1}^{d-1} \omega_{k,l} |k\rangle \langle e_l| + \frac{\Omega_a(t)}{2} |a\rangle \langle e_{d-1}| + \text{H.c.} \quad (13)$$

is a direct extension of Eq. (1). As before, the relation between the number of excited states and qudit ground states is chosen so as to define a single fixed dark eigenstate  $|\mathcal{D}\rangle$ . The coupling structure has the following pattern: the  $l$ th excited state  $|e_l\rangle$  is connected to ground states  $|1\rangle, |2\rangle, \dots, |l+1\rangle$ , except the one with the largest index  $l = d - 1$ , which is connected to all ground states and the auxiliary state  $|a\rangle$ . Thus,  $\omega_{k>l+1,l} = 0$ . Just as in the qutrit case discussed above, dipole transitions between hyperfine levels in trapped ions is the ideal platform for implementing  $H^{(d)}$ .

Let us write the dark state fully residing in the computational subspace as

$$|\mathcal{D}\rangle = c_1|1\rangle + c_2|2\rangle + c_3|3\rangle \cdots + c_d|d\rangle. \quad (14)$$

This defines  $d - 1$  bright states  $|b_k\rangle$  of the form

$$\begin{aligned} |b_1\rangle &= \frac{1}{|c_1|^2 + |c_2|^2} (-c_2^*|1\rangle + c_1^*|2\rangle), \\ |b_2\rangle &= N_2(c_1|1\rangle + c_2|2\rangle + \Lambda_3|3\rangle), \\ &\vdots \\ |b_{d-1}\rangle &= N_{d-1}(c_1|1\rangle + \cdots + c_{d-1}|d-1\rangle + \Lambda_d|d\rangle). \end{aligned} \quad (15)$$

with  $N_2, \dots, N_{d-1}$  being normalization factors. By construction,  $|b_1\rangle$  is orthogonal to the dark state and all other bright states. For  $k \geq 2$ ,  $|b_k\rangle$  contains  $k + 1$  basis vectors, where the coefficient  $\Lambda_{k+1}$  is chosen such that  $|b_k\rangle$  is orthogonal to  $|\mathcal{D}\rangle$ . This in turn makes any  $|b_{l>k}\rangle$  orthogonal to  $|b_k\rangle$  as they have the same states and coefficients as  $|\mathcal{D}\rangle$  for all the states involved in the inner product, which implies that  $\langle b_{l>k}|b_k\rangle \propto \langle \mathcal{D}|b_k\rangle$ . Therefore, by choosing the  $\Lambda$ 's such that these inner products are zero, the construction ensures an orthonormal

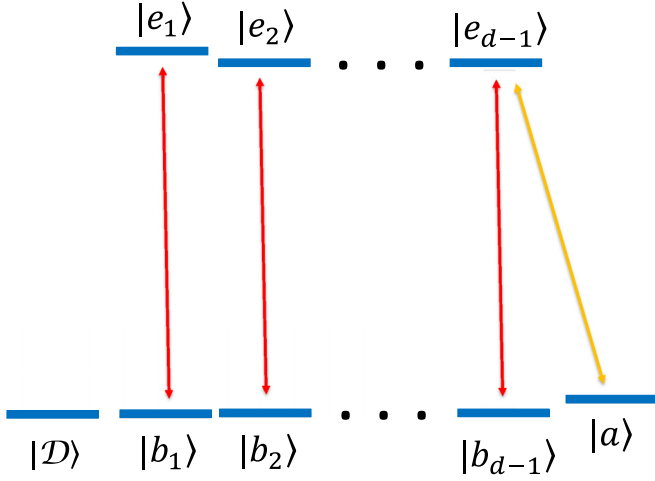


FIG. 6. Qudit setting in the Morris-Shore basis [30] applied to the qudit levels  $|1\rangle, \dots, |d\rangle$ . As in the qutrit case, the auxiliary state  $|a\rangle$  is untouched and a single dark state  $|D\rangle$  emerges in the computational qudit subspace  $\text{Span}\{|1\rangle, \dots, |d\rangle\}$ .

dark-bright basis spanning the qudit subspace. Explicitly, for  $k \geq 2$ , one finds

$$\Lambda_{k+1} = -\frac{1}{c_{k+1}^*} \sum_{l=1}^k |c_l|^2 \quad (16)$$

and

$$N_k = \left( \sum_{l=1}^k |c_l|^2 + |\Lambda_{k+1}|^2 \right)^{-1/2} \\ = \left[ \sum_{l=1}^k |c_l|^2 + \frac{1}{|c_{k+1}|^2} \left( \sum_{l=1}^k |c_l|^2 \right)^2 \right]^{-1/2}. \quad (17)$$

In the dark-bright basis, the Hamiltonian can be written as

$$H^{(d)} = \sum_{k=1}^{d-1} \frac{\Omega_k(t)}{2} e^{-i\phi_k} |b_k\rangle\langle e_k| + \frac{\Omega_a(t)}{2} |a\rangle\langle e_{d-1}| + \text{H.c.}, \quad (18)$$

with  $\Omega_k$  being real-valued time-dependent Rabi frequencies and  $\phi_k$  time-independent phases. This form of  $H^{(d)}$  is depicted in Fig. 6 and can be used to define  $d-1$  independent dark paths  $|D_k(t)\rangle$ ; as above, these states must satisfy  $\langle D_k(t)|H_d|D_k(t)\rangle = 0, k = 1, \dots, d-1$ , and  $\langle D_k(t)|D_l(t)\rangle = \delta_{kl}$ . The dark paths are traced out by the states

$$|D_k(t)\rangle = \cos u(t) e^{-i\phi_k} |b_k\rangle + i \sin u(t) |e_k\rangle, \\ k = 1, \dots, d-2, \\ |D_{d-1}(t)\rangle = \cos u(t) \cos v(t) e^{-i\phi_{d-1}} |b_{d-1}\rangle - i \sin u(t) |e_{d-1}\rangle \\ - \cos u(t) \sin v(t) |a\rangle, \quad (19)$$

each of which starts and ends in one of the bright states provided  $u(\tau) = u(0) = v(\tau) = v(0) = 0$ . By using these states, one can reverse engineer the Hamiltonian to determine  $\Omega_k$  and

$\Omega_a$ , yielding

$$\Omega_1(t) = \Omega_2(t) = \dots = \Omega_{d-2}(t) = -2\dot{u}, \\ \Omega_{d-1}(t) = 2(\dot{v} \cot u \sin v + \dot{u} \cos v), \\ \Omega_a(t) = 2(\dot{v} \cot u \cos v - \dot{u} \sin v). \quad (20)$$

Holonomic one-qudit gates can be implemented by using the same  $u(t), v(t)$  as in the qutrit setting and by using the single-loop multipulse technique [31]. This results in the gate

$$U_d^{(1)} = |D\rangle\langle D| + \sum_{k=1}^{d-1} e^{i\gamma_k} |b_k\rangle\langle b_k| \quad (21)$$

acting on the qudit subspace  $\text{Span}\{|D\rangle, |b_1\rangle, \dots, |b_{d-1}\rangle\}$ . The unitary is parameterized by  $3(d-1)$  parameters for  $d \geq 2$ , i.e.,

$$U_d^{(1)} = U_d^{(1)}(\theta_1, \dots, \theta_{d-1}, \varphi_1, \dots, \varphi_{d-1}, \gamma_1, \dots, \gamma_{d-1}), \quad (22)$$

where we have assumed the  $c_k$ 's are parameterized by the Euclidean components of the radius of the unit  $(d-1)$  sphere with added phase factors:

$$c_1 = \cos \theta_1, \quad c_2 = e^{i\varphi_1} \sin \theta_1 \cos \theta_2, \quad \vdots \\ c_{d-1} = e^{i\varphi_{d-2}} \sin \theta_1 \dots \sin \theta_{d-2} \cos \theta_{d-1}, \\ c_d = e^{i\varphi_{d-1}} \sin \theta_1 \dots \sin \theta_{d-2} \sin \theta_{d-1}. \quad (23)$$

By applying the holonomy with different parameters in sequence up to  $n$  times is enough to create any desirable gate. To determine  $n$ , we use that the qudit state space is isomorphic to the special unitary group  $\text{SU}(d)$ . By using  $\dim[\text{SU}(d)] = d^2 - 1$ , we deduce that  $n$  must satisfy  $3(d-1)n \geq d^2 - 1$ , which implies  $n \geq \frac{d+1}{3}$ . Thus, the number of loops needed to create any unitary scales linearly since some gates can be created with fewer loops. In particular,  $n = \frac{d+1}{3}$  when  $d = 3j + 2, j \in \mathbb{N}$ , which are optimal qudit dimensions in the sense that they require the smallest number of loops per dimension, and these qudits could therefore be regarded as optimal carriers of information since the same number of loops must be carried out while higher dimension has higher information capacity.

Furthermore, any diagonal gate only requires one loop. Explicitly, by setting  $\theta_1 = \dots = \theta_{d-1} = \varphi_1 = \dots = \varphi_{d-1} = 0$  the unitary reduces to the form

$$U_d^{(1)}(0, \dots, 0, \gamma_1, \dots, \gamma_{d-1}) = |1\rangle\langle 1| + \sum_{k=2}^d e^{i\gamma_k} |k\rangle\langle k|. \quad (24)$$

This corresponds to the choice  $c_k = \delta_{k1}$ .

## V. HOLONOMIC DARK PATH TWO-QUDIT GATES

To complete the set of universal gates, we demonstrate a conditional dark path based holonomic gate that can entangle pairs of qudits. The scheme is adapted to trapped ions with their internal states encoding qudits interacting via the vibrations in the harmonic trap. Similar schemes have been developed for standard nonadiabatic holonomic quantum computation [33,34].

A conditional qudit gate has the generic form

$$U_d^{(2)} = \begin{pmatrix} I_{d^2-d} & \\ & V_d \end{pmatrix}, \quad (25)$$

with  $V_d$  a unitary acting on the target qudit provided the control qudit is in the state  $|d\rangle$ . The  $(d^2 - d) \times (d^2 - d)$  identity matrix  $I_{d^2-d}$  acts on the remaining states of the qudit pair.  $U_d^{(2)}$  can be realized by designing the effective Hamiltonian

$$\begin{aligned} \mathcal{H}_{\text{eff}}^{(d)} &= |d\rangle\langle e_{d-1}| \otimes \left( \sum_{k=1}^d \sum_{l=1}^{d-1} \omega_{k,l} |k\rangle\langle e_l| + \frac{\Omega_a(t)}{2} |a\rangle\langle e_{d-1}| \right) \\ &+ \text{H.c.} = |d\rangle\langle e_{d-1}| \otimes H^{(d)} + \text{H.c.}, \end{aligned} \quad (26)$$

which, upon use of the multipulse single-loop technique [31] applied to the dark path, implies that

$$U_d^{(2)} = \mathcal{T} e^{-i \int_0^t \mathcal{H}_{\text{eff}}^{(d)} dt'} = (\hat{1} - |d\rangle\langle d|) \otimes \hat{1} + |d\rangle\langle d| \otimes U_d^{(1)}, \quad (27)$$

with  $\mathcal{T}$  time ordering and  $U_d^{(1)}$  given by Eq. (21).

The effective Hamiltonian in Eq. (26) can be implemented in a Sørensen-Mølmer-type [35] setup, where the single-ion transitions are driven by two-color lasers, all with the same detuning  $\Delta$  to the red and blue of the corresponding resonance frequency. By denoting the single-ion Rabi frequencies as  $\omega_0$  for the control ion and as  $\omega_1, \dots, \omega_N, \omega_a, N = \frac{1}{2}(d^2 + d) - 1$ , for the target ion, we obtain the Hamiltonian

$$\begin{aligned} \mathcal{H}^{(d)} &= i\eta_L (b e^{-i\nu t} + b^\dagger e^{i\nu t}) \otimes [\omega_0(t) |d\rangle\langle e_{d-1}| \otimes \hat{1} \\ &+ \hat{1} \otimes (\omega_1 |1\rangle\langle e_1| + \omega_2 |2\rangle\langle e_1| + \omega_3 |1\rangle\langle e_2| + \dots \\ &\dots + \omega_N |d\rangle\langle e_{d-1}| + \omega_a |a\rangle\langle e_{d-1}|)] \cos \Delta t \\ &+ \text{H.c.} \end{aligned} \quad (28)$$

responsible for the qudit-qudit interaction. Here,  $b$  ( $b^\dagger$ ) is the annihilation (creation) operator of the vibrational mode with frequency  $\nu$  and  $\eta_L$  is the Lamb-Dicke parameter satisfying the Lamb-Dicke criterion  $\eta_L \ll 1$ . In the large detuning limit, single-ion transitions are strongly suppressed and one may use the technique developed in Ref. [36] to derive the effective Hamiltonian

$$\tilde{\mathcal{H}}_{\text{eff}}^{(d)} = \mathcal{H}_{\text{eff}}^{(d)} + \tilde{\mathcal{H}}_{\text{eff}}^{(d)} \quad (29)$$

with

$$\begin{aligned} \tilde{\mathcal{H}}_{\text{eff}}^{(d)} &= -|d\rangle\langle e_{d-1}| \otimes \left( \sum_{k=1}^d \sum_{l=1}^{d-1} \omega_{k,l}^* |e_l\rangle\langle k| + \frac{\Omega_a^*(t)}{2} |e_{d-1}\rangle\langle a| \right) \\ &+ \text{H.c.} \end{aligned} \quad (30)$$

up to Stark shift contributions that can be compensated for by applying additional laser pulses. Here,

$$\begin{aligned} \omega_{1,1} &= k |\omega_0 \omega_1| e^{i\phi_1}, \quad \omega_{1,2} = k |\omega_0 \omega_2| e^{i\phi_2}, \dots, \\ \omega_{d,d-1} &= k |\omega_0 \omega_N| e^{i\phi_N}, \quad \Omega_a = 2k |\omega_0 \omega_a| e^{i\phi_a} \end{aligned} \quad (31)$$

with

$$k = \eta_L^2 \frac{\nu}{\Delta^2 - \nu^2}, \quad \omega_j = |\omega_j| e^{i(\phi_j - \phi_0)}, \quad j = 0, 1, \dots, N, a. \quad (32)$$

We note that  $\tilde{\mathcal{H}}_{\text{eff}}^{(d)}$  commutes with  $\mathcal{H}_{\text{eff}}^{(d)}$ , which implies

$$\mathcal{T} e^{-i \int_0^t \tilde{\mathcal{H}}_{\text{eff}}^{(d)} dt'} = \mathcal{T} e^{-i \int_0^t \mathcal{H}_{\text{eff}}^{(d)} dt'} \mathcal{T} e^{-i \int_0^t \tilde{\mathcal{H}}_{\text{eff}}^{(d)} dt'}. \quad (33)$$

The second factor of the right-hand side of Eq. (33) acts trivially on the computational subspace  $\text{Span}\{|kl\rangle, k, l = 1, \dots, d\}$ , thus effectively reducing  $\tilde{\mathcal{H}}_{\text{eff}}^{(d)}$  to  $\mathcal{H}_{\text{eff}}^{(d)}$ .

As a final remark, up to the laser pulses needed to compensate for Stark shifts, there is only one additional laser needed to implement  $U_d^{(2)}$  as compared to  $U_d^{(1)}$ . Thus, the resources to implement the one- and two-qudit holonomic gates are roughly the same.

## VI. CONCLUSIONS

We have shown how to explicitly create a quantum mechanical system, which could be used to emulate a qutrit and corresponding universal set of one-qutrit holonomic gates. This is done by expanding the dark path qubit scheme [21] into three dimensions. We have shown how it generalizes in the one- and two-qudit case and how the use of auxiliary states can improve the robustness of the gates.

The qutrit gates have high fidelity and their robustness is improved by the inclusion of the auxiliary state in a similar way as for the qubit, which suggests that the dark path method can be beneficial for higher-dimensional qudits to improve robustness. In the general qudit case, we have shown how any one-qudit diagonal unitary could be created by a single multipulse loop in parameter space and that nondiagonal unitaries scale linearly in the number of loops required for control of each loop. The possibility that the scheme expands efficiently into certain dimensions has been discussed.

## ACKNOWLEDGMENTS

E.S. acknowledges financial support from the Swedish Research Council (VR) through Grant No. 2017-03832.

- [1] P. Zanardi and M. Rasetti, Holonomic quantum computation, *Phys. Lett. A* **264**, 94 (1999).
- [2] E. Sjöqvist, D. M. Tong, L. M. Andersson, B. Hessmo, M. Johansson, and K. Singh, Non-adiabatic holonomic quantum computation, *New J. Phys.* **14**, 103035 (2012).
- [3] F. Wilczek and A. Zee, Appearance of Gauge Structure in Simple Dynamical Systems, *Phys. Rev. Lett.* **52**, 2111 (1984).

- [4] J. Anandan, Non-adiabatic non-Abelian geometric phase, *Phys. Lett. A* **133**, 171 (1988).
- [5] J. Zhang, S. J. Devitt, J. Q. You, and F. Nori, Holonomic surface codes for fault-tolerant quantum computation, *Phys. Rev. A* **97**, 022335 (2018).
- [6] G. F. Xu, D. M. Tong, and E. Sjöqvist, Path-shortening realizations of nonadiabatic holonomic gates, *Phys. Rev. A* **98**, 052315 (2018).

- [7] B.-J. Liu, X.-K. Song, Z.-Y. Xue, X. Wang, and M.-H. Yung, Plug-and-Play Approach to Nonadiabatic Geometric Quantum Gates, *Phys. Rev. Lett.* **123**, 100501 (2019).
- [8] S. Li, T. Chen, and Z.-Y. Xue, Fast holonomic quantum computation on superconducting circuits with optimal control, *Adv. Quantum Technol.* **3**, 2000001 (2020).
- [9] W. Dong, F. Zhuang, S. E. Economou, and E. Barnes, Doubly geometric quantum control, *PRX Quantum* **2**, 030333 (2021).
- [10] Y.-H. Chen, W. Qin, R. Stassi, X. Wang, and F. Nori, Fast binomial-code holonomic quantum computation with ultra-strong light-matter coupling, *Phys. Rev. Res.* **3**, 033275 (2021).
- [11] Y. Dong, C. Feng, Y. Zheng, X.-D. Chen, G.-C. Guo, and F.-W. Sun, Fast high-fidelity geometric quantum control with quantum brachistochrones, *Phys. Rev. Res.* **3**, 043177 (2021).
- [12] F. Setiawan, P. Groszkowski, H. Ribeiro, and A. A. Clerk, Analytic design of accelerated adiabatic gates in realistic qubits: General theory and applications to superconducting circuits, *PRX Quantum* **2**, 030306 (2021).
- [13] G. O. Alves and E. Sjöqvist, Time-optimal holonomic quantum computation, *Phys. Rev. A* **106**, 032406 (2022).
- [14] Y. Xu, W. Cai, Y. Ma, X. Mu, L. Hu, T. Chen, H. Wang, Y. P. Song, Z.-Y. Xue, Z.-q. Yin, and L. Sun, Single-Loop Realization of Arbitrary Nonadiabatic Holonomic Single-Qubit Quantum Gates in a Superconducting Circuit, *Phys. Rev. Lett.* **121**, 110501 (2018).
- [15] Y.-Y. Huang, Y.-K. Wu, F. Wang, P.-Y. Hou, W.-B. Wang, W.-G. Zhang, W.-Q. Lian, Y.-Q. Liu, H.-Y. Wang, H.-Y. Zhang, L. He, X.-Y. Chang, Y. Xu, and L.-M. Duan, Experimental Realization of Robust Geometric Quantum Gates with Solid-State Spins, *Phys. Rev. Lett.* **122**, 010503 (2019).
- [16] D. J. Egger, M. Ganzhorn, G. Salis, A. Fuhrer, P. Müller, P. Kl. Barkoutsos, N. Moll, I. Tavernelli, and S. Filipp, Entanglement Generation in Superconducting Qubits Using Holonomic Operations, *Phys. Rev. Appl.* **11**, 014017 (2019).
- [17] Y. Xu, Z. Hua, Tao Chen, X. Pan, X. Li, J. Han, W. Cai, Y. Ma, H. Wang, Y. P. Song, Z.-Y. Xue, and L. Sun, Experimental Implementation of Universal Nonadiabatic Geometric Quantum Gates in a Superconducting Circuit, *Phys. Rev. Lett.* **124**, 230503 (2020).
- [18] Y. Dong, S.-C. Zhang, Y. Zheng, H.-B. Lin, L.-K. Shan, X.-D. Chen, W. Zhu, G.-Z. Wang, G.-C. Guo, and F.-W. Sun, Experimental Implementation of Universal Holonomic Quantum Computation on Solid-State Spins with Optimal Control, *Phys. Rev. Appl.* **16**, 024060 (2021).
- [19] K. Xu, W. Ning, X.-J. Huang, P.-R. Han, H. Li, Z.-B. Yang, D. Zheng, H. Fan, and S.-B. Zheng, Demonstration of a non-Abelian geometric controlled-NOT gate in a superconducting circuit, *Optica* **8**, 972 (2021).
- [20] J.-L. Wu, S. Tang, Y. Wang, X.-S. Wang, J.-X. Han, C. Lü, J. Song, S. L. Su, Y. Xia, and Y.-Y. Jiang, Unidirectional acoustic metamaterials based on nonadiabatic holonomic quantum transformations, *Sci. China Phys. Mech. Astron.* **65**, 220311 (2022).
- [21] M.-Z. Ai, S. Li, R. He, Z.-Y. Xue, J.-M. Cui, Y.-F. Huang, C.-F. Li, and G.-C. Guo, Experimental realization of nonadiabatic holonomic single-qubit quantum gates with two dark paths in a trapped ion, *Fundam. Res.* **2**, 661 (2022).
- [22] M. Glusker, D. M. Hogan, and P. Vass, The ternary calculating machine of Thomas Fowler, *IEEE Ann. Hist. Comput.* **27**, 4 (2005).
- [23] N. P. Brusentsov and J. R. Alvarez, Ternary computers: The Setun and the Setun 70, in *Perspectives on Soviet and Russian Computing*, edited by J. Impagliazzo and E. Proydakov, **357**, 74 (2011).
- [24] B. P. Lanyon, M. Barbieri, M. P. Almeida, T. Jennewein, T. C. Ralph, K. J. Resch, G. J. Pryde, J. L. O'Brien, A. Gilchrist, and A. G. White, Simplifying quantum logic using higher-dimensional Hilbert spaces, *Nat. Phys.* **5**, 134 (2009).
- [25] T. Bækkegaard, L. B. Kristensen, N. J. S. Loft, C. K. Andersen, D. Petrosyan, and N. T. Zinner, Realization of efficient quantum gates with a superconducting qubit-qutrit circuit, *Sci. Rep.* **9**, 13389 (2019).
- [26] Y. Chi, J. Huang, Z. Zhang, J. Mao, Z. Zhou, X. Chen, C. Zhai, J. Bao, T. Dai, H. Yuan, M. Zhang, D. Dai, B. Tang, Y. Yang, Z. Li, Y. Ding, L. K. Oxenløwe, M. G. Thompson, J. L. O'Brien, Y. Li *et al.* A programmable qudit-based quantum processor, *Nat. Commun.* **13**, 1166 (2022).
- [27] Y. Wang, Z. Hu, B. C. Sanders, and S. Kais, Qudits and high-dimensional quantum computing, *Front. Phys.* **8**, 589504 (2020).
- [28] V. O. Shkolnikov and G. Burkard, Effective Hamiltonian theory of the geometric evolution of quantum systems, *Phys. Rev. A* **101**, 042101 (2020).
- [29] P. J. Low, B. M. White, A. A. Cox, M. L. Day, and C. Senko, Practical trapped-ion protocols for universal qudit-based quantum computing, *Phys. Rev. Res.* **2**, 033128 (2020).
- [30] J. R. Morris and B. W. Shore, Reduction of degenerate two-level excitation to independent two-state system, *Phys. Rev. A* **27**, 906 (1983).
- [31] E. Herterich and E. Sjöqvist, Single-loop multiple-pulse nonadiabatic holonomic quantum gates, *Phys. Rev. A* **94**, 052310 (2016).
- [32] L. F. Shampine and M. W. Reichelt, The MATLAB ODE Suite, *SIAM J. Sci. Comput.* **18**, 1 (1997).
- [33] P. Z. Zhao, G. F. Xu, and D. M. Tong, Nonadiabatic holonomic multiqubit controlled gates, *Phys. Rev. A* **99**, 052309 (2019).
- [34] G. F. Xu, P. Z. Zhao, E. Sjöqvist, and D. M. Tong, Realizing nonadiabatic holonomic quantum computation beyond the three-level setting, *Phys. Rev. A* **103**, 052605 (2021).
- [35] A. Sørensen and K. Mølmer, Quantum Computation with Ions in Thermal Motion, *Phys. Rev. Lett.* **82**, 1971 (1999).
- [36] D. F. V. James and J. Jerke, Effective Hamiltonian theory and its applications in quantum information, *Can. J. Phys.* **85**, 625 (2007).